Enhanced Coherent Emission of Terahertz Radiation by Energy-Phase Correlation in a Bunched Electron Beam

A. Doria, G. P. Gallerano,* E. Giovenale, G. Messina, and I. Spassovsky

Ente per le Nuove Tecnologie l'Energia e l'Ambiente (ENEA), UTS Tecnologie Fisiche Avanzate, Sezione Laser ed Acceleratori, P.O. Box 65, 00044 Frascati, Italy

(Received 19 March 2004; published 28 December 2004)

We report the first observation of enhanced coherent emission of terahertz radiation in a compact free electron laser. A radio-frequency (rf) modulated electron beam is passed through a magnetic undulator emitting coherent radiation at harmonics of the rf with a phase which depends on the electron drift velocity. A proper correlation between the energy and phase distributions of the electrons in the bunch has been exploited to lock in phase the radiated field, resulting in over 1 order of magnitude enhancement of the coherent emission.

DOI: 10.1103/PhysRevLett.93.264801 PACS numbers: 41.60.Cr

Until recently, the terahertz spectral range, defined as the frequency interval between 100 GHz and 10 THz (i.e., a wavelength between 3 mm and 30 μm), was considered a rather poorly explored region at the boundary between the microwave and the infrared regions. Frequencies in the terahertz region were usually considered as too high for electronic devices, due to the technological limits in reducing the size of components as frequency increases, and too low for photonic devices, since the corresponding photon energy is comparable to that of thermal excitations at room temperature. This situation has changed during the past few years with a rapid development of coherent sources, such as the quantum cascade laser [1], diodes [2], optically pumped solid state devices [3], and novel free electron devices [4], which is now stimulating a wide variety of applications [5], from material science to telecommunications and from biology to biomedicine.

Free electron devices, such as klystrons, traveling wave tubes (TWTs), and gyrotrons, have been used since the mid-1950s to generate coherent radiation in the millimeter wave region of the spectrum [6]. In klystrons and TWTs, an electron beam transforms its kinetic energy into a radiation field in suitably loaded resonant cavities with the size of the order of the wavelength. To overcome the necessity of reducing the physical size of such devices as the frequency is increased, different schemes have been developed to let the electrons exchange momentum and to allow photon emission. The most frequently used one is the so-called magnetic undulator, a device consisting of an alternate disposition of magnets along the beam propagation axis producing transverse oscillations of the electrons, which is employed in free electron lasers (FELs) [7]. Other free electron devices are the Cherenkov FEL, based on the interaction with a dielectric loaded waveguide [8], and the metal grating FEL, based on the Smith-Purcell effect [9].

In all free electron devices, the coherence of the emitted radiation directly comes from the coherence that can be induced in the electrons generating the electromagnetic wave. A first degree of coherence is obtained when the electrons are bunched along the direction of propagation on a scale comparable to the wavelength of the radiation to be generated [10,11]. When this is realized, at least a fraction N of the electrons in the bunch are approximately seen by the field as a single particle having a charge Q equal to N times the charge e of the electron, and the intensity I of the radiation emitted is $I \propto Q^2 = N^2 e^2$: this is the well known coherent spontaneous emission (CSE). For electrons randomly distributed in phase over a bunch much longer than the wavelength the emission is $I \propto N e^2$. In a radio-frequency (rf) modulated electron beam, a further degree of coherence can be introduced by assigning to each individual electron a value of energy γ_i that is correlated to its longitudinal phase ψ_i. In this case, it is possible to evaluate the effects of different distributions of the electrons in the phase space on the emission process taking place in an undulator. It has been shown [12] that constructive interference is achieved when the electrons are distributed in the phase space (ψ, γ) as close as possible to a so-called "phase-matching" curve. An emission increase, over 1 order of magnitude higher than the one obtained with a prebunched but uncorrelated electron beam, can be expected when the distribution approaches the "ideal" line in the phase space.

This method of enhancing the coherent emission has been successfully tested on the Compact Advanced Terahertz Source (FEL-CATS) at the ENEA laboratories in Frascati, Italy. The layout of the experimental setup, which occupies a floor space of about 1×2 m^2, is shown in Fig. 1. The electron beam source is a 2.998 GHz rf linear accelerator (LINAC) capable of generating an electron current of 250 mA in 5 to 10 μs macropulses at a kinetic energy of about 2.5 MeV [13]. The electron macropulse is composed of a train of 15 ps bunches spaced at the rf period of 330 ps. The electron beam is generated by a pulsed triode gun, equipped with a 7.7 mm diameter osmium treated dispenser thermoionic cathode and is accelerated

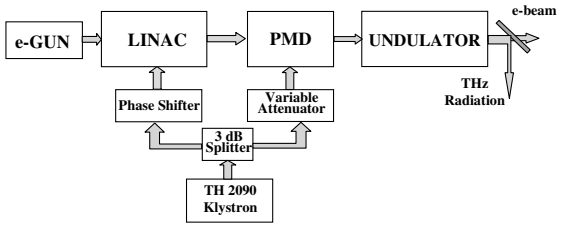

FIG. 1. Schematic layout of the experimental apparatus.

to the 13 kV anode potential before entering the LINAC structure through a magnetic lens assembly. The electrons, after having been accelerated in the LINAC, enter into a second rf section, called the phase-matching device (PMD), where the correlation in the longitudinal phase space takes place. The rf system has been described in detail in [13]: A 15 MW TH2090 klystron followed by a 3 dB power splitter is used to feed both the LINAC and the PMD. A variable attenuator is placed before the PMD to control the rf input power. The LINAC rf line is equipped with a high-power phase shifter, which allows continuous adjustment of the rf phase difference between the LINAC and the PMD from 0° to 360°. The PMD section is placed 4 cm downstream of the LINAC output. The drift space and the phase shift of the PMD are set to have the reference electron passing through the center of the PMD at the zero crossing of the rf field. The PMD is composed of three on-axis coupled cavities (one and two halves) operating in the $\pi/2$ mode. Both the LINAC and the PMD are tuned at the same frequency [13]. The distribution of the bunched electrons in the phase space at the PMD output can be modified by varying the phase and the amplitude of the rf field driving the PMD with respect to the LINAC. A total rf power of about 2 MW is required to run both devices. Two sets of steering coils and a triplet of quadrupoles transport the ''energy-phase correlated'' electron bunch to the undulator entrance. The undulator is a 40 cm long permanent magnet linear device. It is realized with NdFeB magnets in the Halbach configuration, and it consists of 16 periods of 2.5 cm each. The gap is variable and can be remotely controlled to vary the undulator parameter $K = eB_0\lambda_u/(2\sqrt{2}\pi m_0 c^2)$ between 0.5 and 1.4. The results discussed in this Letter refer to an undulator gap of 1.1 cm corresponding to $K = 0.7$ and to an on-axis peak magnetic field of 4.2 kG. The terahertz radiation is generated in a rectangular waveguide with cross-section dimensions $a \times b = 24.67 \times 6.32$ mm^2 placed inside the undulator. Immediately after the undulator, a copper horn, matched to the waveguide cross section, and a 45° copper-mesh reflector launch the terahertz radiation into a copper circular light pipe with 2.5 cm clear aperture. The spent electron beam passes through the mesh reflector and is sent into a beam dump. At the end of the light pipe, the radiation is analyzed by means of a Fabry-Perot (FP) interferometer equipped with mesh reflectors and a pyroelectric detector (Molectron P4-35).

Once the LINAC acceleration is set, the electron energy at the PMD output depends on both the phase difference between the LINAC and the PMD and the microwave power directed to the PMD. To evaluate the electron energy, a simple experimental setup based on the measurement of the electron range in aluminum has been utilized. It consists of two aluminum targets collecting electrons and directing the respective currents I_1 and I_2 toward the ground through 50 Ω resistors. The first target has a thickness of 3.8 mm, corresponding to a cutoff kinetic energy of 2.14 MeV, according to the semiempirical formula [14]: $E(\mathrm{MeV}) = (\rho t + 0.106)/0.530$, where ρ is the material density in g/cm^3 and t the target thickness in cm. The second target is 25 mm thick and can stop electrons with energy below 5 MeV. The two targets can be remotely inserted into the beam path. By integrating the Bethe-Bloch equation for the energy loss of electrons in aluminum for every ratio $R = I_2/I_1$ of the collected currents I_1 and I_2, the corresponding energy value can be determined. A maximum electron energy of 3.4 MeV has been measured in this way by varying the high-power rf attenuator in the PMD waveguide line and the relative rf phase between the LINAC and the PMD. Figure 2 shows the dependence of the electron energy on the PMD rf power at the zero-crossing phase and at the maximum accelerating phase. As can be seen from the figure, no significant variation of the electron energy at the PMD exit is observed at the zero-crossing phase, while at the maximum accelerating phase the measured energy at the PMD exit follows the expected logarithmic dependence on the rf attenuation.

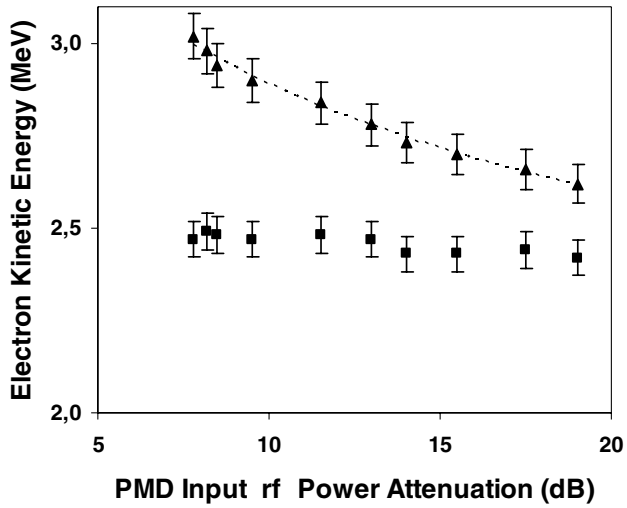

FIG. 2. Measured electron kinetic energy as a function of the relative power attenuation in the PMD for two different phase values. Squares: zero-crossing phase corresponding to the maximum emitted power of Fig. 4; triangles: maximum accelerating phase corresponding to the highest emission frequency (see also Fig. 7). The dotted line shows a logarithmic fit of the measured data.

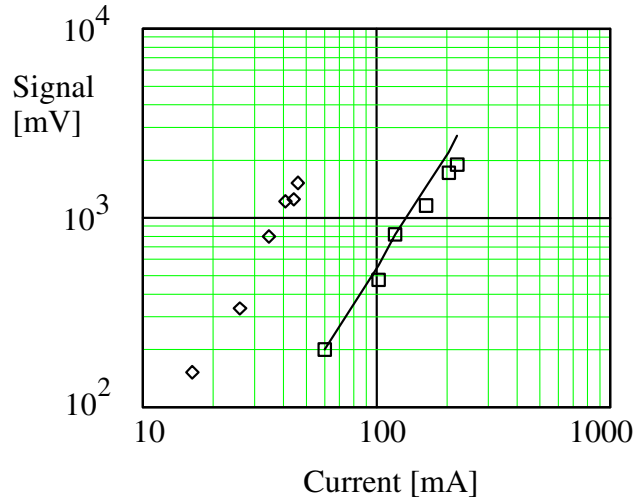

FIG. 3 (color online). P4-35 signal as a function of the electron current collected by the upstream (squares) and downstream (diamonds) targets, respectively. The straight line shows the expected quadratic dependence.

At the start of each run, the electron energy and the relative phase between LINAC and PMD are set according the procedure described above. To analyze the coherence of the emitted radiation, the signal of the pyroelectric detector has been recorded as a function of the e-beam current measured at the entrance and at the beam dump downstream of the undulator. The result is shown in Fig. 3 in a double logarithmic scale; the output power clearly increases as the square of the e-beam current, confirming the occurrence of CSE. Because of the presence of the waveguide and the terahertz launching system, the current collected by the beam dump is only a fraction of the current transported through the undulator; the latter one has actually been measured to be 85% of the injected current. The record of the electron current upstream and downstream of the undulator guarantees that the e-beam transport efficiency is approximately constant during the measurement.

The signal of the pyroelectric detector at maximum transported current is subsequently monitored and optimized by adjusting the PMD phase around the zero crossing, as described before. The dependence of the emitted power as a function of the relative phase between LINAC and PMD is shown in Fig. 4 together with the predicted behavior discussed in [15]. The experimental data fit quite well with the theory for decelerating (negative) values of the phase, while the measured emission is generally higher than the calculated one at accelerating values of the phase. This could be due to the presence of harmonics of the fundamental frequency not yet included in the model.

By scanning the P4-35 detector with a 5 mm aperture across the terahertz beam cross section and integrating the intensity distribution, a maximum emitted power of about 1.5 kW in a 5 μs pulse duration has been measured at the

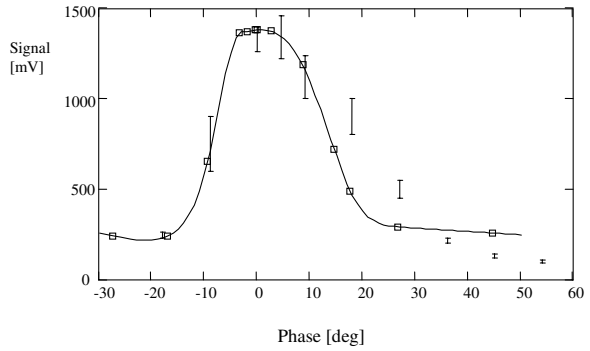

FIG. 4. P4-35 signal (vertical bars) measured as a function of the rf relative phase between LINAC and PMD. Squares show the expected power at selected values of the phase according to [12,15]. The continuous line is the spline interpolation of the calculated data.

peak of the phase-tuning curve when the rf field in the PMD (E_{PMD}) was set to about 0.5 the field in the LINAC (E_{LINAC}). The dramatic increase in the emitted power is shown in Fig. 5, where two FP interferograms, taken at $E_{\mathrm{PMD}} = 0.2E_{\mathrm{LINAC}}$ and $E_{\mathrm{PMD}} = 0.5E_{\mathrm{LINAC}}$, respectively, are compared. The two spectra show the same central peak position, confirming that the mean electron energy is unchanged at zero crossing. The spectrum taken at $E_{\mathrm{PMD}} = 0.5E_{\mathrm{LINAC}}$, however, shows a peak intensity of about a factor 50 higher than the one at $E_{\mathrm{PMD}} = 0.2E_{\mathrm{LINAC}}$. This is ascribed to a higher correlation in phase of the field radiated by the electrons in the bunch, which has been produced by a rotation of the particle distribution in the longitudinal phase space. A slight increase in the spectral bandwidth is also observed at maximum power, indicating an increased energy spread of the correlated electrons. A direct measurement of the corresponding

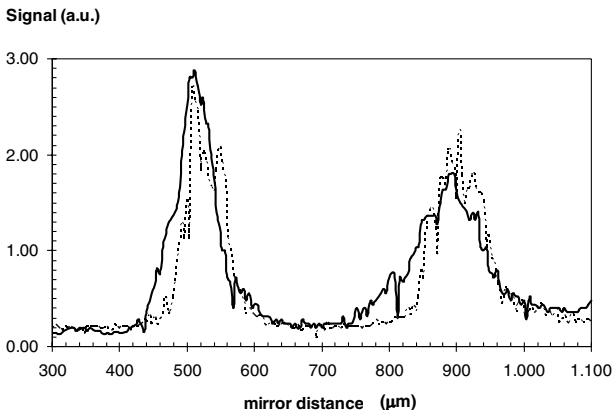

FIG. 5. Comparison of FP interferograms of the terahertz emission at the zero-crossing phase for two different values of the rf field in the PMD (see text). Signal in arbitrary units. Solid line: $E_{\mathrm{PMD}} = 0.5E_{\mathrm{LINAC}}$; dotted line: $E_{\mathrm{PMD}} = 0.2E_{\mathrm{LINAC}}$ (signal amplitude has been magnified $\times 50$ to be compared with the solid line).

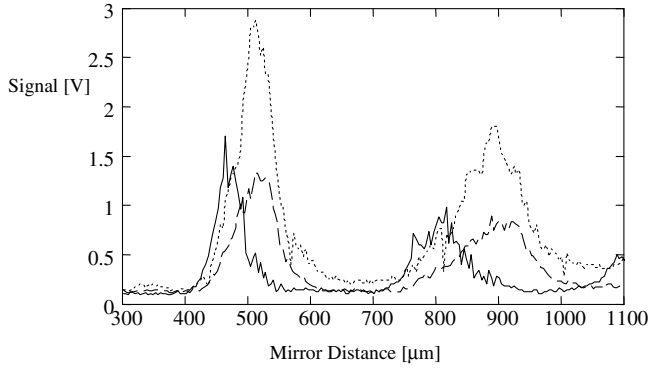

FIG. 6. FP interferograms of the emission at different values of the PMD phase $\Delta\theta$: dotted line, $\Delta\theta = 0$ (zero crossing); dashed line, $\Delta\theta = +9°$; solid line, $\Delta\theta = -9°$.

electron distribution in the longitudinal phase space has been planned as discussed in [13].

It is important to stress that the reported power level has been obtained after a single pass of the electron through the undulator without any optical cavity. The central wavelength of the emission in these operating conditions is 760 μm (0.4 THz); the FP interferogram shows a well shaped spectrum with a relative bandwidth of about 10% (continuous line of Fig. 5). The FP interferometer was equipped with 200 lines/in. and 400 lines/in. mesh reflectors. The finesse of the instrument was calculated to be $F = 22$ at $\lambda = 700$ μm and was enough to resolve a structure within the output bandwidth due to the emission at discrete frequencies, which are the integer harmonics of the 3 GHz rf [10].

Easy and reproducible wide band tunability of FEL-CATS has been achieved by varying the phase in the PMD as it is shown in Fig. 6, where three interferograms demonstrate operation between 600 and 800 μm (0.4–0.5 THz). As the phase is varied, the requirement on the energy-phase correlation is gradually released and the mean kinetic energy of the e beam is either increased or decreased. This results in the emission at a different frequency and, in general, at a lower power level, as is observed from the graphs. Further tunability up to 0.7 THz was obtained by increasing the power in the PMD to get an electron kinetic energy of about 3 MeV. The corresponding FP spectrum is reported in Fig. 7, which shows a central wavelength of 450 μm.

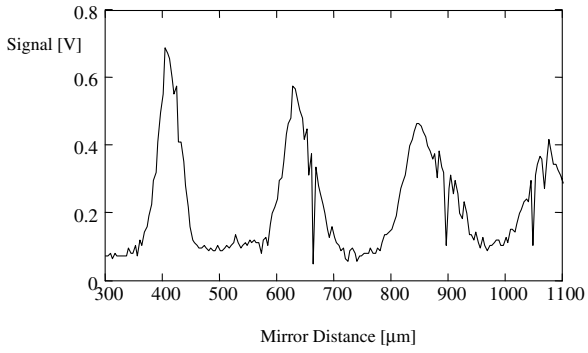

FIG. 7. FP interferogram at maximum rf power and maximum accelerating phase ($-18°$) in the PMD.

Enhanced coherent emission of terahertz radiation in a compact free electron laser has been proven with this experiment by applying a proper correlation between the energy and phase distributions of the electrons in the bunch. The device realized to obtain such a correlation of the electron distribution in the longitudinal phase space also provides a simple and powerful method of tuning the central frequency of the emission. A maximum measured emitted power of 1.5 kW has been obtained without the use of any optical resonator. This power level is only a factor of 5 lower than the maximum saturated power $P_{\mathrm{SAT}} = P_e/4N_u$, where P_e and N_u are the electron beam power and the number of undulator periods, respectively, obtainable in an FEL operated as an oscillator with the same electron beam and undulator parameters. Operation at higher values of the electron current is needed for a further investigation of the saturation process.

We gratefully acknowledge the technical and valuable assistance of M. Bortoli, A. Fastelli, and R. Grossi. We would also like to thank M. D'Arienzo for his precious help in the calibration of the rf system.

*Corresponding author.
Electronic address: gallerano@frascati.enea.it

[1] R. Koehler *et al.*, Nature (London) **417**, 156 (2002).
[2] H. Heisele, A. Rydberg, and G. I. Haddad, IEEE Trans. Microwave Theory Tech. **48**, 626 (2000).
[3] L. Xu, X. C. Zhang, and D. H. Auston, Appl. Phys. Lett. **61**, 1784 (1992).
[4] G. L. Carr *et al.*, Nature (London) **420**, 153 (2002).
[5] P. H. Siegel, IEEE Trans. Microwave Theory Tech. **50**, 910 (2002).
[6] H. Motz, J. Appl. Phys. **22**, 527 (1951); S. H. Gold and G. S. Nusinovich, Rev. Sci. Instrum. **68**, 3945 (1997).
[7] G. Dattoli, A. Renieri, and A. Torre, *Free Electron Laser Theory and Related Topics* (World Scientific, Singapore, 1993).
[8] F. Ciocci *et al.*, Phys. Rev. Lett. **66**, 699 (1991).
[9] G. Doucas *et al.*, Phys. Rev. ST Accel. Beams **5**, 072802 (2002).
[10] A. Doria, R. Bartolini, J. Feinstein, G. P. Gallerano, and R. H. Pantell, IEEE J. Quantum Electron. **29**, 1428 (1993).
[11] F. Ciocci *et al.*, Phys. Rev. Lett. **70**, 928 (1993).
[12] A. Doria *et al.*, Phys. Rev. Lett. **80**, 2841 (1998).
[13] A. Doria *et al.*, Nucl. Instrum. Methods Phys. Res., Sect. A **475**, 296 (2001).
[14] W. J. Whitehouse and J. L. Putman, *Radioactive Isotopes* (Oxford University Press, London, 1953), p. 79.
[15] A. Doria *et al.*, *Proceedings of the European Particle Accelerator Conference, 1998* (IOP Publishing, Bristol, 1998), p. 661.